Low-Profile 3D Microelectrodes with Near-Uniform Current Density for High-Resolution Neural Stimulation

Denys Nikolayev, Wout Joseph, Emmeric Tanghe, Marleen Welkenhuysen, Carolina Mora Lopez, Thomas Tarnaud, Luc Martens

PROCEEDINGS #63: LOW-PROFILE 3D MICROELECTRODES WITH NEAR-UNIFORM CURRENT DENSITY FOR HIGH-RESOLUTION NEURAL STIMULATION

Denys Nikolayev [1,2], Wout Joseph [1], Emmeric Tanghe [1], Marleen Welkenhuysen [2], Carolina Mora Lopez [2], Thomas Tarnaud [1], Luc Martens [1]. [1] *INTEC, imec/Ghent University, 9052 Ghent, Belgium;* [2] *imec, 3001, Heverlee, Belgium*

Abstract

Background: Uniform current density electrodes can reduce the risk of electrode corrosion and tissue damage, but existing geometries do not suit thin planar leads.
Objectives: This study examines current density distribution (CDD) on low-profile electrode designs and proposes an approach to obtain optimal geometries with near-uniform CDD requiring reduced recession depths.
Methods: The electrodes are defined as parametric curves, analyzed using the quasi-static approach, and optimized using the downhill simplex method.
Results: Obtained electrode designs with near-uniform CDD remain low profile and require twice as less recession depths comparing to reference designs.
Conclusion: These electrode shapes are suitable for miniature high-resolution planar DBS leads.

Introduction

Deep brain stimulation (DBS) is an established technique helping us to improve lives and to study the brain. Miniature high-resolution planar shanks [1] are a promising technology that can increase the spatial precision of DBS and hence lessen DBS-induced side effects. However, due to the small electrode surface sizes ($S \lessapprox 10^4$ μm^2), the volume of tissue activated (VTA) is usually insufficient. From the point of view of electric field E and potential V distribution in electrolytes, one can effectively represent any microelectrode as a point source at distances as little as 50 μm [2] (cellular level). For a given electrode surface area, VTA depend mainly on the amount of charge that can be safely injected into electrolyte through capacitive transfer and reversible faradic reactions [3].
The electrode shape affects the spatial distribution of current density |J| on the electrode surface that is a cofactor with charge in stimulation induced neural damage [4]. Under stationary conditions, any planar electrode–insulator pair has a non-uniform charge and thus |J| distributions with their maximums at the electrode edges (Fig. 1A). This may lead to localized electrode corrosion or tissue burns at the edges (Fig. 1B) [3]. A few studies quantified how the electrode shape affect its performance and safety [5–8]. However, to the best of our knowledge, none of these studies focused on electrode shapes for thin planar shanks. Uniformizing |J| distributions can help maximizing the effectiveness of neural stimulation while avoiding tissue damage [9].
A few fundamental shapes give uniform |J| over their surfaces: a conductive sphere, a conductive half-sphere over an infinite insulator, and a disc electrode that is infinitely recessed into an insulator. However, these approaches are incompatible with thin planar shanks (thickness ~ 20 μm). A

more appropriate solution was proposed by Ksienski in [10]. It combines a spheroid-like shape of radius a recessed into a substrate to a depth $d = 0.2077a$ (Fig. 1C–E). Still, to ensure the uniform CDD on electrodes of a 100-μm-wide lead ($a \approx 45$ μm), $d = 9.3$ μm remains unacceptable due to manufacturing and mechanical constraints. Consequently, the maximum recession depth should be limited to a few μm.

In this paper, we characterize, at first, the effect of radius a on the average current density |J| of Ksienski's electrodes on a finite-sized planar shank in order to establish the reference values of |J|. Next, using optimization methods, we develop electrodes with near-uniform current density distributions (CDD) that require reduced (1–3 μm for $a = 45$ μm) recession depths.

Methods

We use a quasi-static formulation [11] in cylindrical coordinates (r, φ, z) to study the current density J over the electrodes using the fully *hp*-adaptive finite element method (*hp*-FEM) [12]. Considering the axial symmetry of the studied electrodes (e.g. Fig. 1E), we reduce the spatial dimensionality of the problem to R^2 [i.e. potential $V(\varphi) = \text{const.}$]. The brain tissue is assumed to have homogeneous and isotropic properties with the conductivity $\sigma = 0.1$ S·m^{-1}.

The Laplace's equation $\nabla \cdot \mathbf{J}(r, z) = 0$ governs distributions of the potential V, electric field $\mathbf{E} = -\nabla V$, and the current density $\mathbf{J} = (\sigma + j\omega\varepsilon_0\varepsilon_r)\mathbf{E}$, where ω is the angular frequency and $\varepsilon_0 \approx 8.85 \times 10^{-12}$ F·m^{-1}. A unitary potential $V_0 = 1$ (V) models the electrode that extends up to a radius $r < a$ (Fig. 1C). The Neumann boundary condition $\mathbf{n} \cdot \mathbf{J} = 0$ represents the perfect insulator ($r \geq a$). A quadrant of a radius $r = 20a$ truncates the computational domain with a Dirichlet boundary condition $V = 0$ (Fig. 1C). To avoid the singularity in the model (Fig. 1D), we round the corner formed by the insulator with a radius of $0.05d$.

The electrode and the shank are defined as analytic curves and optimized numerically to achieve uniform current density (UCD) distributions. Cubic Bézier curves [13] model the electrode surface spanning between the starting point $(r = 0, z = 0)$, and the ending point $(a, -d)$. The starting point is normal to the z-axis. Therefore, four parameters a, e_z, e_r, and c_r (Fig. 1D) define the parametric space for each Bézier curve section. We study electrodes containing n [from one (Fig. 1D) to four] Bézier sections. A 2-μm-thick wall of insulator separates the sections. The curve shape is optimized in terms of $\Sigma_n (a, e_z, e_r, c_r)_n$ using the downhill simplex method in order to achieve the near-uniform CDD. Considering that the charge is conserved [14], we set the objective to minimize the $\max_a|\mathbf{J}|$.

Results and Discussion

First, we characterize a widely used square planar electrode of area 10^4-μm^2 and 1-μm thickness for reference purposes. Fig. 1A shows the charge density distribution over the electrode for $V_0 = 1$ V (the edges are beveled with a radius of 0.3 μm to avoid singularity). Indeed, we see the under-utilization of the electrode surface with the charge stored and being injected mostly from the vertices. The distribution of non-reversible redox currents agrees well with CDD (Fig. 1B).

On the other hand, |J| of a planar disk electrode peaks uniformly at the edge; max|J| is about one order of magnitude lower than for the square electrode of the same 10^4-μm^2 surface area. Yet, the edge-to-center ration of |J| is about nine.

The current density induced by a UCD electrode [$|\mathbf{J}|(r) = \text{const.}$, SD < 0.1%] depends on its radius a (Fig. 1F) and can be accurately predicted as $|\mathbf{J}|$ [A·cm^{-2}] $= 10.31a[\mu\text{m}]^{-0.947}$ (adj. $R^2 = 0.9997$). However, for sufficiently large electrodes ($a > 15$ μm), this design requires recession depths $d > 3$ μm that exceed the capabilities of the manufacturing process. Therefore, we optimize the UCD design ($a = 45$ μm, Fig. 1E) by splitting it into n concentric sections of radii a_n separated by two-μm-thick insulators. The obtained surface is then optimized in terms of $\Sigma_n(a, e_z, e_r, c_r)_n$ using the downhill simplex method that minimizes max|J|.

Fig. 1G compares an optimized shape ($n = 2$, $d = 2.3$ μm, 2-μm-wide insulator at $a_1 = 27$ μm) to a UCD and a planar disk designs of the same radius. Peak |J| = 0.54 A·cm^{-2} is a 74% decrease comparing to a disk electrode, but about twice that of the UCD. The optimized design could be realized on a miniature high-resolution planar shank, as it requires $d \lesssim 3$ μm. The effect of the proposed electrodes on safe charge injection limits is to be characterized in future studies.

References

[1] Lopez CM, Putzeys J, Raducanu BC, Ballini M, Wang S, Andrei A, et al. A neural probe with up to 966 electrodes and up to 384 configurable channels in 0.13 μm SOI CMOS. IEEE Trans Biomed Circuits Syst 2017;11:510–22. doi:10.1109/TBCAS.2016.2646901.

[2] Gimsa J, Habel B, Schreiber U, Rienen U van, Strauss U, Gimsa U. Choosing electrodes for deep brain stimulation experiments–electrochemical considerations. J Neurosci Methods 2005;142:251–65. doi:10.1016/j.jneumeth.2004.09.001.

[3] Merrill DR, Bikson M, Jefferys JGR. Electrical stimulation of excitable tissue: design of efficacious and safe protocols. J

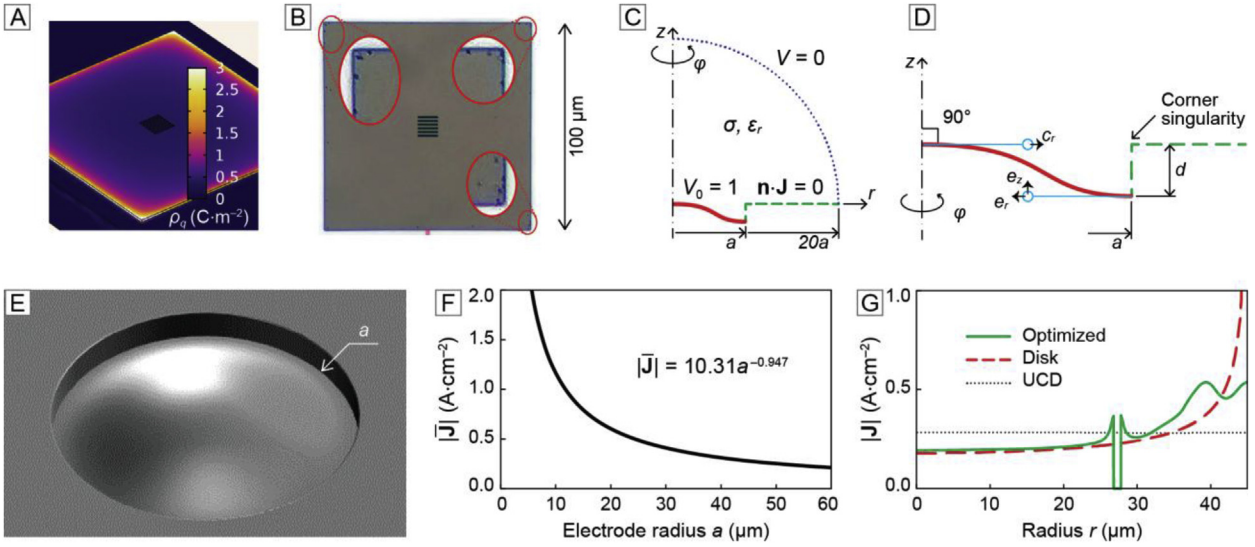

Figure 1. Electrodes for a planar high-resolution DBS lead ($V_0 = 1$ V). **a**. Surface charge density ρ_q distribution over a square $S = 10^4$ μm^2 electrode. **b**. Microphotograph of a 10^4-μm^2 TiN electrode corroded at edges due to voltage-transient measurements *in vitro* [max(I) = 1 mA]. The pattern of damage agrees well with ρ_q or, equivalently, |**J**| distributions. **c**. Formulation of the problem. **d**. Definition of the electrode geometry and parameters. **e**. UCD electrode of radius a recessed to a depth $d = 0.2077a$ [10]. **f**. Average current density |**J**| of a UCD electrode depends on radius a. **g**. Current density distributions over radial components of $a = 45$ μm electrodes: optimized ($d = 2.3$ μm, max|**J**| = 0.54 A·cm^{-2}), disk (max|**J**| = 2.1 A·cm^{-2}), and UCD [10] (d = 9.3 μm).

Neurosci Methods 2005;141:171–98. doi:10.1016/j.jneumeth.2004.10.020.
[4] McCreery DB, Agnew WF, Yuen TG, Bullara L. Charge density and charge per phase as cofactors in neural injury induced by electrical stimulation. IEEE Transactions on Biomedical Engineering 1990;37:996–1001.
[5] McIntyre CC, Grill WM. Finite element analysis of the current-density and electric field generated by metal microelectrodes. Annals of Biomedical Engineering 2001;29:227–35. doi:10.1114/1.1352640.
[6] Wei XF, Grill WM. Current density distributions, field distributions and impedance analysis of segmented deep brain stimulation electrodes. J Neural Eng 2005;2:139–47. doi:10.1088/1741-2560/2/4/010.
[7] Butson CR, McIntyre CC. Role of electrode design on the volume of tissue activated during deep brain stimulation. J Neural Eng 2006;3:1–8. doi:10.1088/1741-2560/3/1/001.
[8] Howell B, Grill WM. Evaluation of high-perimeter electrode designs for deep brain stimulation. J Neural Eng 2014;11:046026. doi:10.1088/1741-2560/11/4/046026.
[9] Wang B, Petrossians A, Weiland JD. Reduction of edge effect on disk electrodes by optimized current waveform. IEEE Trans Biomed Eng 2014;61:2254–63. doi:10.1109/TBME.2014.2300860.
[10] Ksienski DA. A minimum profile uniform current density electrode. IEEE Trans Biomed Eng 1992;39:682–92. doi:10.1109/10.142643.
[11] Bossetti CA, Birdno MJ, Grill WM. Analysis of the quasi-static approximation for calculating potentials generated by neural stimulation. J Neural Eng 2008;5:44. doi:10.1088/1741-2560/5/1/005.
[12] Karban P, Mach F, Kůs P, Pánek D, Doležel I. Numerical solution of coupled problems using code Agros2D. Computing 2013;95:381–408. doi:10.1007/s00607-013-0294-4.
[13] Farin G. Algorithms for rational Bézier curves. Computer-Aided Design 1983;15:73–7. doi:10.1016/0010-4485(8390171-9).
[14] Jackson JD. Classical electrodynamics. 3rd ed. Hoboken, NJ: John Wiley & Sons; 1999